

Hall-Effect Evolution across a Heavy-Fermion Quantum Critical Point

Silke Paschen¹, Thomas Lühmann, Steffen Wirth, Philipp Gegenwart, Octavio Trovarelli², Christoph Geibel, Frank Steglich, Piers Coleman³, and Qimiao Si⁴

Quantum critical points (QCPs) are of great current interest because of their singular ability to influence the finite temperature properties of materials. Recently, heavy-fermion metals have played a key role in the study of antiferromagnetic QCPs. The Fermi surface of the heavy-fermion paramagnet is known to be larger than that of an antiferromagnet [1,2]. An important unsolved question is whether the Fermi-surface transformation at the QCP develops gradually, as expected if the magnetism is of spin-density-wave type [3,4], or suddenly as expected if the heavy electrons are abruptly localized by magnetism [5-7]. Our recent measurements of the low-temperature Hall coefficient R_H in the heavy-fermion metal YbRh_2Si_2 reveal that, upon field-tuning it from an antiferromagnetic to a paramagnetic state, R_H undergoes an increasingly rapid change near the QCP as the temperature is lowered, extrapolating to a sudden jump in the zero temperature limit. We interpret these results in terms of a collapse of the large Fermi surface and of the heavy-fermion state itself precisely at the QCP [8].

YbRh_2Si_2 is particularly well suited to study the evolution of the Hall effect across a QCP. Magnetic susceptibility and specific heat indicate that it orders antiferromagnetically via a second-order phase transition at very low temperatures ($T_N = 70 \text{ mK}$) [9]. The antiferromagnetic nature of the transition is supported by NMR data [10]. The Néel temperature T_N is continuously suppressed down to the lowest experimentally accessed temperatures by application of a small magnetic field ($B_{1c} \approx 0.7 \text{ T}$ for a field along the magnetically hard c -axis, $B_{2c} \approx 60 \text{ mT}$ for a field within the easy tetragonal plane) [11]. Isothermal magnetostriction measurements indicate that the transition remains of second order down to at least 15 mK [12]. Moreover, unlike for several other heavy-fermion compounds [13] (and the high- T_c superconductors), the QCP is not hidden by superconductivity. This is in spite of the high quality of the YbRh_2Si_2 single crystals investigated here (residual resistivities of $\approx 1 \mu\Omega\text{cm}$ [11]).

The Hall effect of YbRh_2Si_2 is surprisingly simple. Outside the quantum critical region the Hall resistivity is linear in field resembling the behavior

of simple metals. Furthermore, an analysis of the temperature-dependent Hall coefficient in terms of the anomalous Hall effect (Fig. 1a) reveals that the low-temperature Hall coefficient (below about 1 K) is dominated by its *normal* contribution [14,15]. These features imply that the low-temperature Hall coefficient can be used as a measure of the Fermi-surface volume.

At zero magnetic field, the data measured at the lowest temperatures tend to saturate at the value of the normal Hall coefficient extracted from the data between 7 K and room temperature (Fig. 1a). This indicates that, at $B = 0$, the Fermi-surface volume is the same at the lowest temperatures as it is at high temperatures. Thus, even though there is evidence for the onset of Kondo screening at approximately 20 K [9,11] and for surprisingly large effective quasiparticle masses in the antiferromagnetically ordered state close to the QCP [11], the local moments do, at the lowest temperatures and at $B = 0$, not appear to be incorporated into the Fermi surface. In the *static* sense [1,2], YbRh_2Si_2 may therefore not be classified as a “heavy-fermion” metal.

In the intermediate temperature range, between approximately 70 mK and 7 K, there is an additional contribution ΔR_H which is not due to the anomalous Hall effect (Fig. 1a). In the main part of Fig. 1b we show that, between 0.7 K and 5 K, the cotangent of the Hall angle, $\cot \Theta_H$, is linear in T^2 (while $\Delta\rho \propto T$), indicating that the longitudinal and transverse scattering rates are different [16]. This type of behavior is well known in high- T_c cuprates where it has been taken as evidence for spin-charge separation[16]. However, the temperature range where this relation holds (inset of Fig. 1b), is narrower than the one where the non-Fermi liquid (NFL) behavior $\Delta\rho \propto T$ is observed (from 100 mK to almost 10 K [11]), even if YbRh_2Si_2 is field-tuned to quantum criticality (green squares in inset).

In our field-dependent Hall-effect measurements on YbRh_2Si_2 the magnetic field plays dual roles, as both a “tuning” and a “probe” field. On the one hand, the coupling between the field and the Yb^{3+} moments tends to align the latter: It is this Zeeman-like coupling which tunes the ground state of the

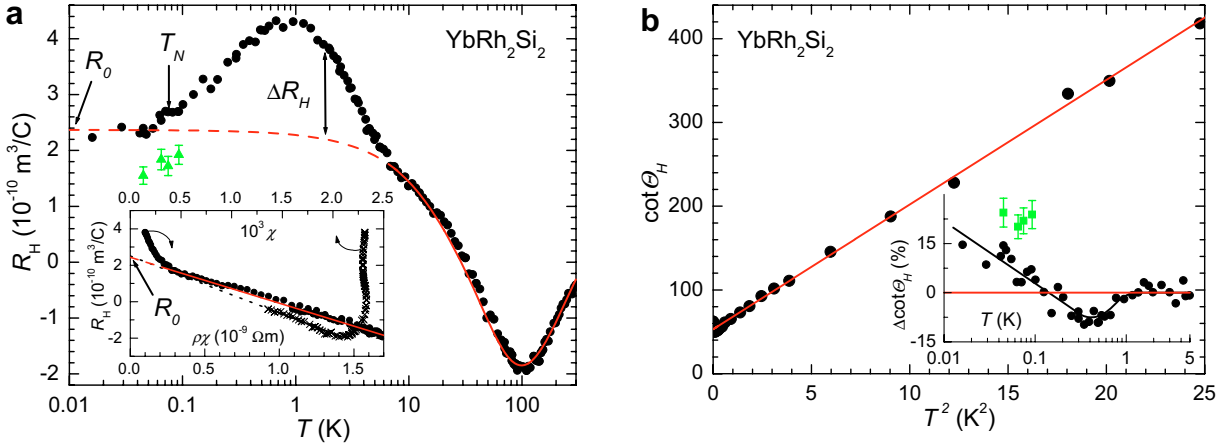


Fig. 1a: Temperature-dependent initial Hall coefficient R_H (T). The green triangles correspond to R_H data obtained from the crossed-field experiment for large values of the tuning field B_2 , suggesting that the Fermi-surface volume is distinctly larger in the field-induced paramagnetic state than in the antiferromagnetic one. Inset: R_H vs product of electrical resistivity ρ and magnetic susceptibility χ (lower axis) and vs χ (upper axis), where temperature is an internal parameter. The full red (black) line is a linear fit accounting for the anomalous Hall effect, the dashed lines are the extrapolations to $T = 0$ (red lines also shown in the main panel).
b: Cotangent of the Hall angle $\cot \Theta_H$ ($\equiv \rho/R_H B$) as a function of T^2 , taken at $B = 1$ T, and linear fit (red line, replotted also in inset). Inset: Difference between data and fit of main panel. The black line is a guide to the eye. Below 0.7 K, the data deviate considerably from the fit. The green squares correspond to $\cot \Theta_H$ data obtained from the crossed-field experiment at the respective crossover fields ($B_2 = B_0$), indicating that, closer to the QCP, these deviations are even stronger.

material, ultimately suppressing the antiferromagnetism and creating the QCP. On the other hand, the magnetic field also generates a weak Lorentz force on the underlying electrons which produces the Hall response. The weak orbital coupling responsible for the Lorentz force does not appreciably change the ground state so that, to a good approximation, we can discuss the two couplings independently. The sample geometry allowed for two distinct types of experiments, “transverse tuning” where the tuning field B_1 is parallel to the c -axis, perpendicular to the current, and “longitudinal tuning” where the tuning field B_2 lies parallel to the current in the basal plane (cf. schematics in Figs. 2a and b). The longitudinal field B_2 produces essentially no Hall response [8] and only serves to tune the state: a separate, crossed probe field ΔB_1 along the c -axis is required to measure the Hall response. In this longitudinal (crossed-field) experiment, the Hall resistivity ρ_H is a direct measure of the field-tuned (linear-response) Hall coefficient $R_H(B_2)$. In the transverse (single-field) case, on the other hand, the magnetic field simultaneously tunes the state and probes the Hall response, and the differential Hall coefficient $\tilde{R}_H(B_1)$ is the sum of an orbital (“probing”) contribution and a Zeeman (“tuning”) contribution. The orbital term is, accord-

ing to the Kubo formalism, just the generalized definition of a Hall coefficient [8], while the Zeeman term is not related to a readily measurable linear-response quantity.

We first discuss the results of the single-field experiment. Figure 2a displays several representative isotherms of the Hall resistivity ρ_H , corrected for its anomalous contribution $\rho_{H,a}(B)$ [8], vs B_1 . $\rho_H - \rho_{H,a}$ shows a linear low- B_1 behavior with larger and a linear high- B_1 behavior with smaller slope. The crossover between the two regimes broadens and shifts to higher B_1 with increasing temperature. For a quantitative analysis of the data we choose $\tilde{R}_H(B) = R_H^\infty - (R_H^\infty - R_H^0)\gamma(B)$ as a fitting function, where R_H^0 is the zero-field Hall coefficient and R_H^∞ is the asymptotic differential Hall coefficient at large fields. $\gamma(B)$ is a crossover function changing from unity at low fields to zero at large fields, which we parameterize as $\gamma(B) = 1/[1+(B/B_0)^p]$. Here, B_0 is the crossover field and p determines the sharpness of the transition, which has a width $\Gamma \sim B_0/p$ when p is large. For $p \rightarrow \infty$, $\int \tilde{R}_H(B) dB$ has a sharp kink at $B = B_0$, corresponding to a step in $\tilde{R}_H(B)$ itself. The fits to the data are shown as solid lines in Fig. 2a. For one temperature the derivative of the fit, corresponding to $\tilde{R}_H'(B_1)$, is shown as well. The crossover fields B_0 obtained from these

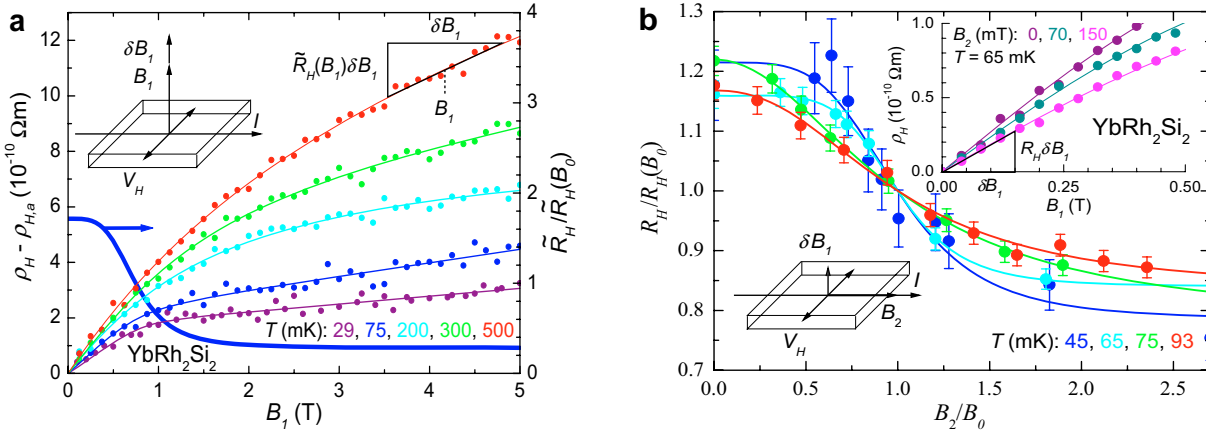


Fig. 2a: Single-field experiment. Typical isotherms of the Hall resistivity ρ_H , corrected for its anomalous contribution $\rho_{H,a}(B)$, vs magnetic field $B_1 = \mu_0 H_1$ ($\parallel c$ -axis). The solid curves represent best fits (see text) to the data. The derivative of the fit at 75 mK is plotted on the right axis.

b: Crossed-field experiment. Initial slope R_H , normalized to its value at the crossover field B_0 , of all measured ρ_H vs B_1 curves as a function of B_2/B_0 , at 45, 65, 75, and 93 mK. The solid lines represent best fits (see text) to the data. Inset: ρ_H vs B_1 curves at three different values of the tuning field $B_2 = \mu_0 H_2$ ($\perp c$ -axis) at 65 mK. The solid lines represent best fits, as in *a*. Similar data have been obtained at the other temperatures (not shown). The sketches in *a* and *b* illustrate the experimental set-up.

fits are included as red dots in the temperature-field ($T - B$) phase diagram of YbRh_2Si_2 (Fig. 3a). A linear fit to these points (dashed red line in Fig. 3a denoted T_{Hall}) extrapolates at zero temperature to the critical field $B_{1c} \approx 0.7$ T for the disappearance of antiferromagnetic order, i.e. to the QCP. Thus, the crossover is directly related to the QCP. The sharpness of the crossover is best quantified by the full width at half maximum (FWHM) of $d\tilde{R}_H/dB_1$, which represents the change of slope of $\rho_H(B_1)$. The temperature dependence of the FWHM values is well described by a *pure* power law, $\text{FWHM} \propto T^a$, $a = 0.5 \pm 0.1$ (inset of Fig. 3a), suggesting that, at zero temperature, the crossover is infinitely sharp (FWHM = 0).

We now turn to the crossed-field measurement of the linear-response Hall coefficient. The inset of Fig. 2b displays $\rho_H(B_1)$ curves taken at 65 mK for different values of the longitudinal tuning field B_2 . With increasing B_2 the linear-response Hall coefficient R_H decreases. For a quantitative analysis we fit, as above, $\int \tilde{R}_H(B) dB$ to the $\rho_H(B_1)$ data (solid lines in the inset of Fig. 2b). As opposed to the single-field experiment, $R_H^0 = R_H$ is now the only parameter to consider. R_H , normalized to its value at the crossover field B_0 , is plotted in the main panel of Fig. 2b as a function of the normalized tuning field B_2/B_0 . Data obtained in the same way at 45 mK, 75 mK, and 93 mK are included as well.

R_H decreases as a function of B_2 by a factor of ≈ 1.5 . In a simple one band model this corresponds to an increase in the charge carrier concentration from ≈ 2 to ≈ 3 holes per YbRh_2Si_2 formula unit on going from the antiferromagnetically ordered state to the paramagnetic, heavy Landau Fermi liquid one. The crossover sharpens up as the temperature is lowered. For a quantitative analysis we may now fit the crossover form $R_H(B) = R_H^\infty - (R_H^\infty - R_H^0)\gamma(B)$ to the $R_H(B_2)$ data (solid curves in main panel of Fig. 2b). The R_H^∞ values obtained for these four temperatures are included as green triangles in the main part of Fig. 1a, showing that the Hall coefficient in the field-induced Landau Fermi liquid (LFL) state (cf. Fig. 3a) at very low temperatures is substantially smaller than in the $B = 0$ antiferromagnetically ordered state. The $11B_0$ and FWHM values obtained from the above fits are included as green dots in Fig. 3a and its inset. The factor of 11 accounts for the fact that the tuning field B_2 is applied in the easy tetragonal plane of YbRh_2Si_2 where, due to the magnetic anisotropy, the action of a magnetic field is known to be ≈ 11 times as strong as along the magnetically hard c -axis [11]. For both quantities the green and red data points agree within the error bars. Thus, the linear Hall response $R_H(B_2)$ of the crossed-field measurement and the differential Hall response $\tilde{R}_H(B_1)$ of the single-field measurement can be described by the

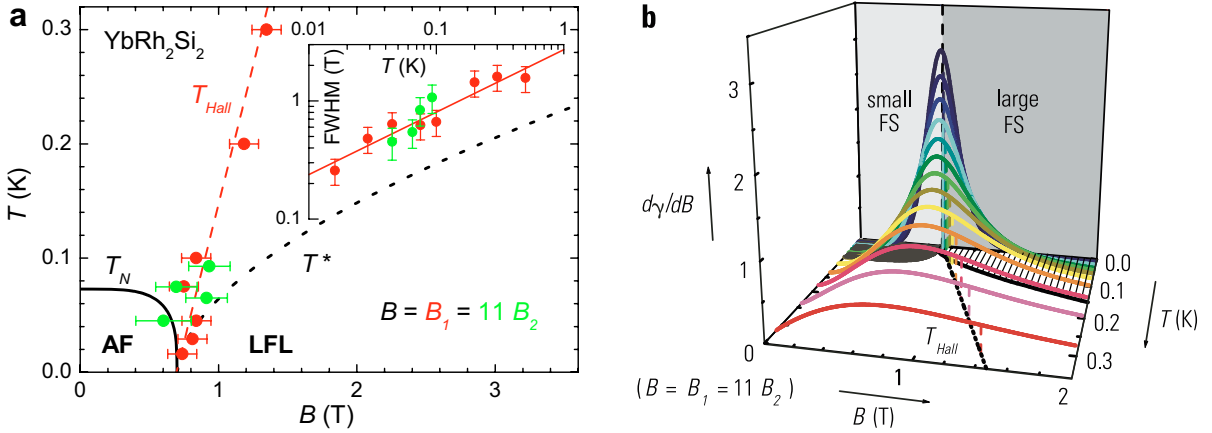


Fig. 3a: Temperature-field phase diagram of YbRh_2Si_2 . The red data points correspond to the B_0 values of the single-field experiment (cf. Fig. 2a). The red dotted line denoted T_{Hall} is the best linear fit to all data up to 0.5 K . It extrapolates at zero temperature to $\approx 0.7 \text{ T}$, the critical field B_{lc} for the direction parallel to the c -axis. The green data points correspond to $11B_0$ determined in the crossed-field experiment (Fig. 2b). The full and dotted black curve represent the field dependence of the Néel temperature T_N and the crossover temperature T^* to a $\Delta\rho \propto T^2$ law, respectively, as determined from iso-field $p(T)$ data [11]. Inset: Full width at half maximum (FWHM) of $\tilde{R}_H(B_1)/dB_1$ in a log-log plot (red points). The red solid line, $\propto T^a$, $a = 0.5 \pm 0.1$, is a best fit to these data. As in the main panel, the green dots correspond to the crossed-field experiment.

b: 3D representation of the field derivative of the crossover function $\gamma(B)$ defined in the text. The colored curves represent arbitrary isotherms of $d\gamma(B)/dB$, obtained using both the $B_0(T)$ fit of *a* and a power law fit to the corresponding $p(T)$ data (not shown). The field B corresponds to $B_1 \parallel c$ or to $11B_2 \perp c$. The positions B_0 are designated by broken drop lines and the black dotted line denoted T_{Hall} in the $T - B$ plane. The antiferromagnetic phase and the region where $\Delta\rho \propto T^2$ are marked as black and hatched areas, respectively, in the $T - B$ plane. At the lowest temperatures, $d\gamma(B)/dB$ may be interpreted as indicating the change of the effective carrier concentration. In the limit $T \rightarrow 0$, $d\gamma(B)/dB$ is a δ -function (dotted line in the $T = 0$ plane), separating the states of small and large Fermi surface (FS) at $B = B_{lc} = 11B_{2c}$.

same functional form and the respective crossover positions and crossover widths agree quantitatively. This experimental finding suggests that the Zeeman term plays a minor role, at least in the experimentally accessed part of the $T - B$ phase diagram. Therefore, here the single-field experiment appears to probe essentially the same (linear-response) Hall coefficient as the crossed-field experiment. However, there is a quantitative difference in the jump heights of $\tilde{R}_H(B_1)$ and $R_H(B_2)$ which probably reflects the anisotropies in the evolution of the electronic bandstructure under transverse and longitudinal field-tuning [17], amplified by the likely presence of a multisheeted, anisotropic Fermi surface.

Figure 3b shows a 3D representation of $d\gamma(B)/dB$ in the magnetic field-temperature parameter space. $\gamma(B)$ is calculated at arbitrary temperatures from the linear B_0 vs T fit (dashed red line in Fig. 3a) and a power law fit (not shown) to the $p(T)$ data obtained from the fits to $\rho_H(B_1)$ (Fig. 2a) and to $R_H(B_2)$ (main panel of Fig. 2b). With decreasing temperature, the $d\gamma(B)/dB$ curves sharpen and their

crossover position B_0 , designated by drop lines, shifts to lower fields such that, at zero temperature, a δ -function (dashed line in $T = 0$ plane in Fig. 3b) is situated at the QCP.

Thus, the extrapolation of the finite temperature data to zero temperature indicates the presence of a finite discontinuity (“jump”) in the Hall coefficient at the QCP, even though the change in the magnetic order parameter is infinitesimal [18]. By contrast, in an itinerant SDW scenario, the Fermi surface is expected [6] to fold over at the QCP; the Hall coefficient is then continuous across the QCP, evolving gradually with the size of the antiferromagnetic order parameter, as is indeed observed experimentally [19]. Our results hint at a sudden reconstruction of the Fermi surface at the QCP, corresponding to the sudden loss of “mobile” $4f$ electrons [6,7,20]. Loosely speaking, the volume of the Fermi surface has changed discontinuously. From our data we infer that the antiferromagnetically ordered ground state has a “small” Fermi surface which is the same as the one extracted from the high-temperature Hall effect data (main panel of Fig. 1a) while the para-

magnetic ground (field-induced heavy Landau Fermi liquid) state has a “large” Fermi surface which presumably counts the new heavy-fermion states injected by the local moments.

The crossover line $T_{Hall}(B)$ (Fig. 3) is then interpreted as the *finite temperature* signature of the “jump” in the Fermi-surface volume. It delineates the position at which a new large Fermi surface emerges in the incoherent electron fluid. Note that $T_{Hall}(B)$ does not follow the antiferromagnetic transition line $T_N(B)$ (Fig. 3a). Indeed, within experimental resolution, the initial Hall coefficient shows no change at the zero field Néel temperature of 70 mK (Fig. 1a). This behavior contrasts dramatically with that expected in an itinerant SDW, where changes in the Hall coefficient should coincide with the Néel transition — as is indeed observed for $\text{Cr}_{1-x}\text{V}_x$ [19,21,22]. Thus we may discard the possibility that the observed crossover in the Hall coefficient of YbRh_2Si_2 is due to a unit-cell doubling in a symmetry breaking antiferromagnetic transition. Even though the crossover at $T_{Hall}(B)$ broadens rapidly with temperature [cf. FWHM(T) in the inset of Fig. 3a and width of $d\gamma(B)/dB$ in Fig. 3b], so that it cannot be followed beyond about 0.5 K, the additional contribution ΔR_H to the initial Hall coefficient (main panel of Fig. 1a) which we attribute to fluctuations of the Fermi-surface volume can be discerned up to much higher temperatures of order 10 K. This is precisely the temperature below which NFL behavior is observed in thermodynamic and dynamical properties [9,11]. This observation makes it very tempting to hold fluctuations of the Fermi-surface volume responsible for the NFL behavior observed over this same temperature window. The fact that the NFL behavior is observed in the entire phase diagram above T_N and T^* (and below 10 K) can be related to the broadness of the crossover.

To summarize we have observed a rapid crossover of the Hall coefficient as function of a control parameter. By extrapolation to $T=0$ of both the Hall crossover and the magnetic phase transition [11], we infer that a large jump of the Hall coefficient occurs at the QCP. We expect this new insight, made possible primarily by the absence of superconductivity, to have broad implications for other strongly correlated electron systems [23].

References

- [1] R. M. Martin, Phys. Rev. Lett. **48** (1982) 362.
- [2] M. Oshikawa, Phys. Rev. Lett. **84** (2000) 3370.
- [3] J. A. Hertz, Phys. Rev. B **14** (1976) 1165.
- [4] A. J. Millis, Phys. Rev. B **48** (1993) 7183.
- [5] A. Schröder, G. Aeppli, R. Coldea, M. Adams, O. Stockert, H. Löhlmeisen, E. Bucher, R. Ramazashvili, and P. Coleman, Nature **407** (2000) 351.
- [6] P. Coleman, C. Pépin, Q. Si, and R. Ramazashvili, J. Phys.: Condens. Matter **13** (2001) R723.
- [7] Q. Si, S. Raballo, K. Ingersent, and J. L. Smith, Nature **413** (2001) 804.
- [8] S. Paschen, T. Lühmann, S. Wirth, P. Gegenwart, O. Trovarelli, C. Geibel, F. Steglich, P. Coleman, and Q. Si, Nature **432** (2004) 881.
- [9] O. Trovarelli, C. Geibel, S. Mederle, C. Langhammer, F. M. Grosche, P. Gegenwart, M. Lang, G. Sparn, and F. Steglich, Phys. Rev. Lett. **85** (2000) 626.
- [10] K. Ishida, K. Okamoto, Y. Kawasaki, Y. Kitaoka, O. Trovarelli, C. Geibel, and F. Steglich, Phys. Rev. Lett. **89** (2002) 107202.
- [11] P. Gegenwart, J. Custers, C. Geibel, K. Neumaier, T. Tayama, K. Tenya, O. Trovarelli, and F. Steglich, Phys. Rev. Lett. **89** (2002) 056402.
- [12] R. Küchler, F. Weickert, P. Gegenwart, N. Oeschler, J. Fersl, C. Geibel, and F. Steglich, J. Magn. Magn. Mater. **272-276** (2004) 229.
- [13] G. R. Stewart, Rev. Mod. Phys. **73** (2001) 797.
- [14] S. Paschen, T. Lühmann, C. Langhammer, O. Trovarelli, S. Wirth, C. Geibel, and F. Steglich, Acta Physica Polonica B **34** (2003) 359.
- [15] S. Paschen, T. Lühmann, S. Wirth, O. Trovarelli, C. Geibel, and F. Steglich, Physica B **359-361** (2005) 44.
- [16] P. W. Anderson, Phys. Rev. Lett. **67** (1991) 2092.
- [17] J. Custers, PhD thesis, TU Dresden, Germany 2004.
- [18] K. Ishida, D. E. MacLaughlin, B.-L. Young, K. Okamoto, Y. Kawasaki, Y. Kitaoka, G. J. Nieuwenhuys, R. H. Heffner, O. O. Bernal, W. Higemoto, A. Koda, R. Kadono, O. Trovarelli, C. Geibel, and F. Steglich, Phys. Rev. B **68** (2003) 184401.
- [19] M. Lee, A. Husmann, T. F. Rosenbaum, and G. Aeppli, Phys. Rev. Lett. **92** (2004) 187201.
- [20] T. Senthil, M. Vojta, and S. Sachdev, Phys. Rev. B **69** (2004) 035111.
- [21] A. Yeh, Y.-A. Soh, J. Brooke, G. Aeppli, T. F. Rosenbaum, and S. M. Hayden, Nature **419** (2002) 459.
- [22] S. Paschen, Physica B (Proc. SCES05) in press.
- [23] F. F. Balakirev, J. B. Betts, A. Migliori, S. Ono, Y. Ando, and G. Boebinger, Nature **424** (2003) 912.

¹ Present address: Vienna University of Technology, Vienna, Austria

² Present address: Infineon Technologies, Dresden, Germany

³ Rutgers University, Piscataway, USA

⁴ Rice University, Houston, USA